

Mapping lamellar organization to the MRI-based hippocampal morphology by an axis-referenced morphometric model

Na Gao¹⁺, Chenfei Ye²⁺, Hantao Chen¹, Xingyu Hao¹, Ting Ma^{123*}

¹The Department of Electronic & Information Engineering, Harbin Institute of Technology (Shenzhen), Shenzhen, China.

²International Research Institute for Artificial Intelligence, Harbin Institute of Technology at Shenzhen, Shenzhen, China.

³Peng Cheng Laboratory, Shenzhen, China.

*These authors contributed equally to this work.

*Corresponding author: Ting Ma. Phone: +86-755-26033608; fax: +86-755-26033608; e-mail: tma@hit.edu.cn

Abstract

The hippocampus is a crucial cognitive center of the human brain and vulnerable to various neurodegenerative diseases. Its longitudinal axis, exhibited as an anterior-posterior gradient, has been discovered differentially interacts with diverse brain systems. However, how to map this gradual transition topography onto the hippocampal morphology has not been well-established, limiting the understanding of extrinsic functional projection and corresponding disease-affected hippocampal lesion progression. To address this issue, we propose a representation of the hippocampal morphology adapted to its lamellar organization, called the axis-referenced morphometric model (ARMM). We first set up a coordinate system on the inscribed medial surface (IMS) within the hippocampus with coordinate lines corresponding naturally to transverse and longitudinal axes through conformal reparameterization. Then, the hippocampal surface is reconstructed referring to this coordinate system by the radial mapping from the local frame of the IMS, forming lamellar distributions perpendicular to the long-axis. Through inverse mapping, the hippocampal surface is unfolded onto a uniform two-dimensional rectangle, facilitating point-wise morphological correspondence across individuals. We evaluate ARMM by comparing the shape representation on a 7T ex-vivo MRI hippocampal atlas with three state-of-the-art models. Results demonstrate the best performance in head folds ($Dice=0.9934$) and long-axis representation. Moreover, ARMM on longitudinal 7T images shows that hippocampal lesions are primarily located in the anterior same lamellae and symmetric superior and posterior during early AD progression. Overall, the ARMM offers a precise anatomically motivated morphometric assessment of the hippocampal longitudinal organization and sheds light on discovering novel image markers for neurodegeneration associated with hippocampal damage.

Keywords: Hippocampus; Morphometrics; Lamellar organization; MRI; Computational anatomy.

1. Introduction

The human hippocampus is a crucial brain structure responsible for memory processing,

learning, spatial navigation and emotions (Chauhan P et al., 2021) and is vulnerable to most neurocognitive diseases (Baazaoui N et al., 2022). Current researches have focused more intensively on the longitudinal organization of the hippocampus since it has been shown to be tightly integrated into large-scale brain networks. How this longitudinal axis accommodates the seemingly disparate functions ascribed to the hippocampus receives much debate. Combining many observations from anatomy, gene expression and function across species, Strange BA et al. (2014) have proposed a model in which a functional long-axis gradient is superimposed on discrete functional domains. Recently, the gradient hypothesis appears to be dominant, as *in vivo* studies have shown that the extrinsic connectivity and gene expression of the human hippocampus follow a gradual pattern along the long-axis (Figure 1; Ayhan F et al., 2021; Dalton MA et al., 2022; Vogel JW et al., 2020). In addition, increasing *in vivo* studies on hippocampal lesions indicate dissociable cognitive function in the anterior versus posterior hippocampus (Bernhardt BC et al., 2016; Dautricourt S et al., 2021; Decker AL et al., 2020; Kalmady SV et al., 2017; Langnes E et al., 2020; Lee JK et al., 2020; Plachti A et al., 2020; Szeszko PR et al., 2003). Reconsidering the hippocampus as a heterogeneous structure along its long-axis can help explain specific behavioral impairments associated with hippocampal damage.

Given that the functional organization of the hippocampus follows a continuous longitudinal gradient, whether the intrinsic anatomy of the hippocampus can provide structural support for this extrinsic manifestation requires to be answered. One hypothesis that has been proposed to address this question involves the lamellar organization of the hippocampus, which suggests that neuronal layers within the hippocampus are arranged along the longitudinal axis, providing anatomical evidence supporting the notion of a gradient-like model in the hippocampus (Andersen P et al., 1969; Andersen P et al., 2000; Pak S et al., 2022; Sloviter RS and Lomo T, 2012). Specifically, the fiber orientations of principal cell axons in the hippocampus are distributed in parallel, forming a thin strip-like fashion oriented nearly perpendicular to the long-axis of the hippocampus. These thin transverse slices, called the lamellae, could represent a functional unit of the hippocampus. The cells in each lamella form the most basic circuit of the hippocampus, called the tri-synaptic circuit, where the information transform from the entorhinal cortex (EC) to the DG to the CA3, CA2, and CA1 before closing the loop back to the SUB and EC. Across lamellae, longitudinal neuron connections in CA1-CA1, CA3-CA3, and DG-DG have been discovered along the long-axis. Under this architecture, a relatively simple structure might exhibit a variety of unique functions in a manner that each functional unit participates in information processing and functional integration through longitudinal connections. We illustrate the lamellae and longitudinal interlamellar connections in the hippocampal body, where the lamellar structures are distributed throughout the entire length of the hippocampus (see Figure 1). Recent studies have discovered more enriched information flow in the longitudinal plane than the transverse plane (Pak S et al., 2022), highlighting the important role of longitudinal connections. It is believed that the malfunction of the lamellar circuits and longitudinal connections is a root cause of aging and neurodegeneration (Irving AJ and Harvey J, 2014; Noh W et al., 2019; Pak S et al., 2022).

The specific location and shape of the lamellar structures on the hippocampus depends on the orientation of its long-axis. The human hippocampus, different from other species,

has expanded anterior and variable gyrfications relative to the posterior, resulting in more complex long-axis curvature, and therefore requires precise delineation. In general, the main curvature on the longitudinal dimension of the human hippocampus follows a typical curved trajectory that forms a "crescent" shape (Genon S et al., 2021). Ding SL and Van Hoesen GW (2015) has inspected the subfields in the uncus, a part of the hippocampal head that curves medially and superiorly to the amygdala, and shows that all subfields continuously follow this curvature throughout the head (Figure 1, crimson line from the posterior to anterior terminating in 'vert. unc'). Adler DH et al. (2018) and Gross DW et al. (2020) also demonstrate quite similar inner architecture along the entire length of the hippocampus, an "interlocking C" profile formed by the principal cell layers of CA and DG (Figure 1, the three-dimensional curved surface of CA and DG). Despite the fact that the number and extent of the small folds, often called digitations (Figure 1), on the hippocampal head vary among individuals, this longitudinal trajectory remains stable. Based on this evidence, we may represent the hippocampal morphology by multiple thin lamellar distributed subdivisions along the entire long-axis of the hippocampus.

However, current morphological models have limitations in representing and measuring this lamellar architecture of the hippocampus in MR images. Image-based shape analysis models, such as SPHARM-PDM (spherical harmonic description point distribution models) and s-reps (skeletal representations) (Styner M et al., 2006; Liu Z et al., 2021), can generate the longitudinal axis of the hippocampus but encounter difficulties in following the complex folds in the head. It is challenging to maintain continuity of internal geometric properties under large local deformation. Also, it is difficult to avoid overlapping of the fan-out lamellae where the cortex folds. Moreover, traditional registration-based methods are unable to provide stable point-wise correspondence across individuals due to the variability of the number of digitations (DeKraker J et al., 2021). The unfolding method described in (DeKraker J et al., 2018) proposes a longitudinal lamellar representation of hippocampal anatomy and a surface-based coordinate system for cross-individual correspondence, but it requires extensive manual labor for each individual hippocampus. The aim of this study is to establish a lamellar representation of the hippocampus based on MRI that can achieve accurate morphological measurement along the long-axis and be used for research on hippocampus-related diseases.

In this paper, we propose an axis-referenced morphometric model (ARMM) to characterize the lamellar organization of the hippocampus based on a hippocampal atlas of 7T ex-vivo MRI and histology (Adler DH et al., 2018). The backbone of the method is to establish an interior coordinate system in the hippocampus with coordinate lines corresponding to longitudinal and transverse axes through conformal mapping. Then, the boundary surface mesh of the hippocampus can be reconstructed from the coordinate system, forming lamellar distributions perpendicular to the long-axis. The inverse mapping enables surface textures to transport from boundary surfaces onto planar coordinates, facilitating the establishment of correspondence across individuals. The ARMM can measure various structural features, including the location, curvature and length of the long-axis, digitations, local thickness and width along the longitudinal and transverse axes, subfield distributions, and surface curvatures. The ARMM reshapes the original uniform-distributed voxel- or vertex-based hippocampus from MRI into a lamellar-distributed morphology

along the entire long-axis. The model is verified by precisely measuring the longitudinal structure of the hippocampus and capturing subtle shape variations by unique structural features on lamellae due to the neurodegeneration. The ARMM offers an anatomically motivated morphological model that has the potential to reveal novel image markers for diseases associated with hippocampal damage. The code for this project, including the ARMM template, is available at <https://github.com/calliegao/ARMM>.

The main contributions of this study include:

- i) We propose an axis-referenced morphometric model to represent the longitudinal lamellar organization of the hippocampus based on a 7T ex-vivo MRI atlas, where the structural features along the long-axis can be precisely quantified.
- ii) The method provides a uniform intrinsic coordinate system by conformally unfolding the hippocampal boundary surface onto two-dimensional plane, allowing for inter-individual hippocampi alignment.
- iii) Local atrophy is observed in the anterior hippocampus during early AD, distributed on the same lamellae and is symmetric superior and posterior.

2. Methods

We aim to characterize the lamellar organization of hippocampal morphology based on MRI. We propose a computational model to represent and measure the longitudinal properties of the hippocampus. Figure 2 outlines the framework of our methodology. Based on an atlas of the hippocampus that captures average anatomy and a series of atlases that capture longitudinal anatomic variabilities corresponding to the transition from nondementia control (NC) to Alzheimer's disease (AD) (Adler DH et al., 2018), we use a two-stage framework. First, we set up an interior coordinate system on the geometric symmetry of the hippocampus, which is represented as an inscribed medial surface (IMS) inside the hippocampus. The centermost longitudinal coordinate line is designated as the long-axis, and the transversal axes are perpendicular to the longitudinal axes with respect to the lamellar architecture. Second, this interior coordinate system is used to reshape the boundary surface representation by applying medial-axis geometric constraints. A conformal mapping is used to unfold the hippocampal surface to a common planar coordinate system. Details of the method are described below.

Data preparation

We employ an atlas of the hippocampus that captures average anatomy derived from a large cohort of ex vivo 7T MRI and histological datasets (Adler DH et al., 2018). The data repository is located at <https://www.nitrc.org/projects/pennhippoatlas/>. The voxel size of the image is 0.2mm × 0.2mm × 0.2mm. The atlas includes 6 hippocampal subfields: cornu ammonis (CA) 1, 2 and 3, stratum radiatum lacunosum moleculare (SRLM), dentate gyrus (DG) and the subiculum (SUB). This atlas is defined as a cross-sectional hippocampal atlas (cHA) and is used as a template that we aim to accommodate (Figure 2a).

A longitudinal hippocampal atlas (IHA) that captures anatomic variabilities corresponding to the transition from nondementia control (NC) to Alzheimer's disease (AD) derived from the same study (Adler DH et al., 2018) is used to verify the performance of our model when characterizing disease-related subtle structural variations. The image series includes 21 images (voxel size: 0.2mm × 0.2mm × 0.2mm). We extract raw surfaces of the hippocampi using ITK-SNAP (Yushkevich PA et al., 2006).

The axis-referenced coordinate system of the hippocampus

The skeleton is a kind of geometric symmetry used to simplify a complex shape. Mathematically, the symmetry axis of the hippocampus can be represented as an internal medial surface by the medial axis geometry (Pizer SM et al., 2022; Siddiqi et al., 2008). We have made some modifications to the medial axis for application in this study, and the details are described in the *Supplementary Material*. One important modification involves smoothly extending the medial surface outward until it reaches the object's boundary surface. This results in an inscribed medial surface (IMS) used to represent the symmetry of the object. Here, we generate the IMS of the template hippocampus in three steps. First, we calculate the Voronoi graph according to the boundary surface of the hippocampus. Second, we create a NURBS surface that best fits the Voronoi points inside the hippocampus. This surface is an approximate medial surface of the hippocampal shape. Finally, we smoothly extend the medial surface to meet the boundary surface of the hippocampus, as shown in Figure 2b.

A rectangular mesh on a two-dimensional plane is conformally mapped to the IMS, where the centermost longitudinal line is manually adjusted to best approximate the intersection between the IMS and the CA-DG border (the CA region includes subfield CA1,2,3 and the DG includes the SRLM). The conformal mapping is performed by methods described in (Meng T W, et al., 2016), with four manually defined landmark vertices on the border of the IMS corresponding to the four corners of the planar rectangle. A reparameterized IMS is illustrated in Figure 2c. Due to the conformal mapping, the transversal (medial-lateral) axes are ensured to be nearly vertical to the longitudinal axes on the IMS. These orthogonal curvilinear coordinate lines serve as a reference to reshape the hippocampal boundary surface.

A radial flow from the reparameterized IMS to the boundary surface of the hippocampus can provide a way to index any position within the hippocampus. We specify the target of the radial flow to be on the boundary surface, and then the radial mapping can be represented as a vector field. These vectors are called "spokes" in medial axis geometry. Let S denote the original surface boundary of the target hippocampus, and \tilde{S} be the reconstructed surface. Spokes on the IMS need to satisfy the following conditions: (1) \tilde{S} should agree with S ; (2) spokes are vertical to the boundary surface; (3) the lengths of superior spokes are equal to the corresponding inferior spokes. We initialize the spokes on the IMS by unit normal vectors on the IMS. Then, we use an iterative scheme to refine the initial spokes. First, to ensure the accuracy of the reconstructed shape, we need condition (1) to strictly hold. Second, we set a proper threshold to measure the non-orthogonality of spokes to the boundary surface, i.e., $1 - \cos(\theta_p)$, where θ_p denotes the angle between the spoke direction at vertex p on the IMS and the normal vector of the boundary surface at the nearest vertex to the spoke tips. Third, because the spokes at bends of the hippocampal head often cross the boundary surface, pointing to wrong places, we solve the problem by enforcing condition (3), then gradually adjust these spokes directions to be approximately orthogonal to the boundary surface. Finally, we iterate above three steps and once more implement condition (1) to get the final refined spokes.

Suppose that the medial surface m is parameterized by (u, v) , and a spoke U is placed at each location $m(u, v)$. Then, any points on the hippocampal surface can be uniquely

indexed by (m, U) in this coordinate system. Figure 2d shows the superior and inferior spokes attached on the IMS of the hippocampus.

Reshaping the boundary surface

Theoretically, the hippocampal boundary surface can be reconstructed by smoothly connecting all spoke tips. However, in digital shape models, it is hard to satisfy all three geometric conditions described above. The self-overlap of spokes will occur at the bending part (e.g., the folds on the hippocampal head), leading to self-intersecting faces on the reconstructed surface mesh. To refine the surface representations, the superior and inferior surfaces are first roughly reconstructed by superior and inferior spokes respectively. The two triangular surface meshes are corrected and subdivided automatically using the *MeshLab* toolkit (Cignoni P et al., 2008). Then, each surface is conformally reparameterized by (u, v) in a two-dimensional rectangular domain. We rearrange the mapped spoke tips to be uniformly distributed on the two-dimensional plane. These inverse mapped spokes can overcome self-overlap at the folds. By connecting the spoke tips that correspond to the same transverse axis, we get a “border” of a “lamellae”, which is ensured to be perpendicular to the long axes on the IMS by the conformal reparameterization. An example refined boundary surface mesh of the hippocampus with 22 lamellae and 2mm intervals is shown in Figure 2e. The thicknesses between each of two neighboring lamellae can be manually designed by implementing interpolation or down-sampling of the spoke density.

Since the conformal mapping builds correspondence between the IMS and the planar rectangle, and the radial mapping corresponds the superior/inferior surfaces and the IMS, subfield distributions and local curvatures on hippocampal boundary surface can be projected onto the two-dimensional plane through these correspondences. This process equals to unfold the hippocampal surface to the two-dimensional plane while remaining the geometric properties of surface textures. An unfolded hippocampal surface is presented in Figure 2f and fitted with a two-dimensional coordinate system. Each straight line of the same u -value in this coordinate system corresponding to a lamella on the hippocampus. When inspecting the topography of the hippocampal subfields, the SRLM forms a typical “C shape” on transverse slices, with subfields CA1, 2, 3, SUB and part of DG cutting off the external dorsal portion of the “C” shape into five parts. The ventral part of the “C” shape consists DG and part of CA3. Therefore, the unfolding of the hippocampal surface keeps topography of subfields that distributes around the external dorsal part of the SRLM, including all the CA1, 2, SUB, most part of CA3, and part of DG. Therefore, through this unfolding, any points on these subfields can be uniquely indexed and identified on the two-dimensional orthogonal coordinate system. By mapping the surfaces of a group of hippocampi, the unfolding onto this uniform rectangle facilitates point-wise morphological correspondence across individuals.

Morphological measurement

The above methods implemented on the cHA form what we call the axis-referenced morphometric model (ARMM) of the hippocampus. Local surface features, such as curvatures quantified by discrete mean curvatures on the mesh vertices, have been widely used and proved to be sensitive to local shape changes. In addition, subfield borders on the hippocampal surface can be projected onto the IMS by conformal correspondence. Volumetric features, such as thickness, width, and bending, which have also shown to be

useful in disease-affected focal locations, can be measured along the coordinate lines of the reparameterized IMS. In this study, distances from mesh vertices to the IMS are defined as local thicknesses. Since the whole hippocampal surface is cut into superior and inferior surface along the fold curve, where the IMS meets the boundary surface, vertices on each of the two surfaces have respective local thickness, called the superior thickness, and the inferior thicknesses. This definition has several advantages: 1) Any vertices on the hippocampal surface, including those with no corresponding spokes, have measurable thickness; 2) The thickness between the superior/inferior surfaces and the IMS is a straight-line/Euclidean distance, which is more easily interpreted than the Laplace thickness (Jones et al., 2000) in terms of a sheet-like shape; 3) Considering thicknesses of superior and inferior portions of the object respectively makes it convenient to study local shape change on each portion. We have summarized all structural features that can be measured by the proposed ARMM and their corresponding descriptions in Table 1.

Model evaluation

The raw hippocampal surface extracted from the label image is used as the ground truth to test the geometric accuracy of the ARMM. The hippocampal surface is reconstructed using four shape models (ARMM, SPHARM-PDM (Styner M et al., 2006), ds-rep (Liu Z et al., 2021) and cm-rep (Yushkevich PA, 2009)) respectively. We test four metrics that measure the accuracy of the reconstructed hippocampi by the shape models, including surface distance, areal difference, curvedness error and dice index. The surface distance Q is defined as

$Q = \frac{1}{n} \sqrt{\sum_{i=1}^n \|p_i - q_i\|^2}$, where n is the number of vertices on surfaces, and p_i, q_i represent the corresponding points on two surfaces. The Euclidean distance $d_i = \|p_i - q_i\|$ ($i = 1, \dots, n$) denotes each point-wise distance. The correspondence related to point-wise distance is constructed by searching for the nearest point between surfaces via the Iterative Closest

Point (ICP) method. The curvedness at each vertex is defined by $c = \sqrt{(k_{\max}^2 + k_{\min}^2)/2}$, where k_{\max} and k_{\min} represent the main curvature. Further, we convert the reconstructed surfaces into binary image labels and rigidly register the labels into the original image label of the template hippocampus, then calculate the dice index between the reconstructed shape and the ground truth. The dice index is defined as $Dice = \frac{2 \times Volume(R \cap G)}{Volume(R) + Volume(G)}$, where R denotes the image label of the reconstructed shape, and G denotes the ground truth label. To evaluate the accuracy of ARMM in shape representation on different portions of the hippocampus, we subdivide the hippocampus into head, body and tail by 1/3 and 2/3 of the anterior-posterior extent. We cut 1/2 of the hippocampal head tip along the medial-lateral orientation, which consists of a fold that curves medially and superiorly. We further cut 1/2 of the hippocampal tail tip along the anterior-posterior orientation.

To automatically generate representations for a group of hippocampi in IHA, we transform the ARMM of the template model to the target hippocampus using a diffeomorphic transformation method provided by the *deformetrica* toolkit (Fishbaugh J et al., 2017). For simplicity, we let each of the images denote a single time point. We first rigidly align all the hippocampi to the baseline hippocampus. Second, we fit the baseline hippocampus with an ARMM using the deformation strategy. Third, hippocampi on each other time point share the same IMS of the baseline hippocampus while optimizing the spokes and fold curves to fit each hippocampus boundary surface. Finally, the boundary

surface on each time point is reconstructed by using the surface reshaping method described above. Local surface variations are quantified by calculating the point-wise surface distance between the baseline and the i^{th} observed surface. The point-wise surface correspondence is established by the coordinate system of ARMMs. Thickness variation is evaluated by subtracting the local superior/inferior thickness measured on each vertex of the reshaped hippocampal surface from the corresponding thickness measured on the baseline hippocampus.

3. Results

Model accuracy

We applied the ARMM to the cHA and compared its accuracy with those of three other shape models (cm-rep, SPHARM-PDM and ds-rep). As presented in Table 2, the results show that the ARMM outperformed the other three models in all portions of the hippocampus in surface distance and dice, particularly in the head fold and tail tip. The areal difference of ARMM is found to be higher than that of SPHARM-PDM, which is expected, given the relatively sparse point distribution on the lateral surface of the hippocampus due to the fan-out lamellae from the lateral to medial. The ARMM also performed the best on the head and tail portions of the hippocampus, as indicated by the results of curvedness and surface area.

Figure 3A visualizes the local surface distance between the reconstructed surfaces and the ground truth. The SPHARM-PDM and ARMM perform well in characterizing the hippocampal head and tail, while the ds-rep and the cm-rep models fail to capture the bending on these two portions. The ARMM shows higher accuracy than SPHARM-PDM, particularly at the bending on the medial side of the head. Lamellar boundaries on the hippocampal surface are generated from the ARMM and visualized as black curves in Figure 3A, showing a fanned-out distribution from the lateral to medial of the hippocampus, with no overlaps at folds (the bending part of the hippocampal head).

Figure 3B shows the long-axis of the hippocampus from the four models. The ds-rep and SPHARM-PDM well characterize the curved body of the hippocampus but fail to capture the bending on the hippocampal head and the end of the tail. The cm-rep cannot generate an explicit longitudinal axis directly from its medial surface. None of the three models consider the interior anatomical structure of the hippocampus. The last panel of Figure 3B shows a 3D visualization of the subfield distribution and the long-axis derived from ARMM, which agrees with the CA-DG border and follows the orientation of the entire longitudinal curvature.

The ARMM in Figure 3B shows a local thickness map measured on the superior hippocampal vertices respecting the reparameterized IMS. The curved transverse and longitudinal coordinate lines are nearly orthogonal to each other on the IMS of ARMM. We have calculated the angular distortion of conformal reparameterizations of the IMS, where the angular distortion refers to the difference between angles of the triangle elements on the 2D rectangle and corresponding angles on the conformal reparameterization. All of the angular distortions are found to be less than one degree, ensuring that the lamellae are perpendicular to the longitudinal axes.

Morphometrics on disease-affected shape variations

We applied the ARMM to the IHA. The features characterizing the shape variations of the hippocampus during the progression of AD are presented in Figure 4. Local surface and thickness variations at four time points (the 6th, 11th, 16th and 21st time points) compared

to the baseline (the 1st time point) hippocampus are displayed in Figure 4a and Figure 4b, which show more severe atrophy on the inferior than the superior during the disease progression. The thickness variations are consistent with the surface distance variations while obviously showing the lamellae of the hippocampal lesions located in. The atrophy initially occurs on the inferior lateral of the body and the tail tip, while focal atrophy is located in the medial head on the same lamella and symmetric superior and inferior. The thickness decreases are diffuse and focally distributed along the long-axis of the hippocampus, gradually spreading from the middle portion of the head to the posterior during AD progression. The primary lesions remain to be on the same lamellae symmetric superior and inferior, with the inferior hippocampus having more severe atrophy.

In the left panel of Figure 4c, the typical locations on the hippocampus that suffer relatively large curvature variations during disease progression are shown. The red points denote where the mean curvature decreases, and blue points denote where the mean curvature increases. These points are distributed near a specific long-axis, the black curve shown on the hippocampal surface. The right panel of Figure 4c shows curvature variations of these points along the longitudinal axis on the 20 observed hippocampi from NC to AD compared to the baseline hippocampus. At the locations where the surface curvature is positive (convex), such as the middle superior of the body and the top of the head, curvature tends to decrease over time. Conversely, at locations where the surface curvature of the surface is negative (concave), such as the superior bending of the head and the lateral tail, curvature tends to increase. The results reflect local atrophy at these locations of the hippocampus.

Figure 4d shows the width variations along the entire long-axis of the hippocampus during disease progression. The left panel of Figure 4d explains how we measure the widths of the hippocampus along the longitudinal curvature of the hippocampus, and the red arrows point to locations where large width decrease occurs. The right panel of Figure 4d shows width variations along the long-axis of the entire hippocampus across the NC to AD progression. Width decreases occur mainly at the portion near the top of the head and the end of tail, while the width near the first bending of the head increases.

Figure 4e illustrates the entire hippocampal length variations. The left panel explains how we measure these lengths, and the red curves are lengths that suffer relatively large variations over disease progression. The diagram on the right shows the lengths variations during NC to AD progression. We find that the lateral of the hippocampus has the greatest length decreases.

4. Discussion

We propose a lamellar representation for the MRI-based hippocampal morphology to capture and measure the longitudinal organization of the hippocampus. An axis-referenced morphometric model (ARMM) is developed based on an existing averaged anatomical atlas derived from 7T MRI and histology (Adler DH et al., 2018). The ARMM establishes an interior coordinate system within the hippocampus to index any location in the hippocampus and reshape the hippocampal boundary surface by lamellar distributions along the entire long-axis. We evaluate the accuracy of ARMM for characterizing the hippocampal shape and its ability to capture shape variations caused by neurodegeneration. In using this model, there are two aspects of the ARMM that need to be highlighted: (1) the reasonability of the

explicit long-axis and lamellae derived by the ARMM, and (2) the stability of point-wise correspondence provided by the ARMM coordinate system. In the following sections, we discuss these aspects and the limitations of our method in detail.

The long-axis and lamellae of the hippocampus derived by ARMM

In this study, the lamellar structures on the surface are determined by transverse axes that are orthogonal to longitudinal axes, where the centermost longitudinal axis follows the intersection between the CA-DG border and IMS. This centermost longitudinal axis is defined as the long-axis of the template hippocampus. Currently, there is no consensus on the location and morphology of the long-axis of the hippocampus. The tripartite model, which subdivides the hippocampus into head, body and tail, as displayed by the red dotted lines shown in Figure 5, is commonly used in image studies. However, recent studies suggest that the entire length of the hippocampus should be considered in morphological analysis. Adler DH et al. (2018) take the medial curvature as the long-axis, while Gross DW et al. (2020) take the lateral curvature as the long-axis.

DeKraker J et al. (2018) propose a method to trace the entire hippocampal length through longitudinal potential field on SRLM by Laplace equation. They demonstrate that the SRLM shape can well capture the general hippocampal shape, including the complex folding patterns on the head. However, the paper also finds that the SRLM is often not visible in the most medial, vertical component of the uncus, which must be manually defined. Large cross-individual differences in the hippocampus should also be considered in the shape model. The different number and scale of digitations on the head and tail cause the lateral/ventral curvature to fluctuate and deviate from the natural curvature of the entire hippocampus. This is also the case for the SRLM. The variable folding patterns will lead to diverse long axes among individuals, which is a disadvantage for population analysis of hippocampal morphology. Therefore, it is not practical to trace the long-axis by tracing the SRLM.

Despite the many uncertainties, we can confirm that the long-axis of the hippocampus has its natural anterior termination in the more medial and superior component of the uncus, and all subfields of the hippocampus contiguously follow this curvature through the hippocampal head (Ding SL and Van Hoesen GW, 2015). Generally, the curvature of the hippocampi on the longitudinal dimension remains a consistent trajectory. For example, the left hippocampus curves like a crescent from posterior to anterior, and curves medially, posteriorly, then superiorly. This trajectory moderates the folding patterns caused by variable digitations, which is more feasible for statistical analysis.

We find that the long-axis generated by the ARMM often lies on the border between CA3 and DG, around the CA3 pyramidal cells that are close to the subgranular zone (SGZ) of DG, except for the portions near the head and tail endpoints. Some evidence supporting the reasonability of this long-axis includes, first, Gross DW et al. (2020) demonstrate the internal subfield consistency inside the hippocampal head. We compare the subfields on slices along the long-axis of our template hippocampus with the subfield distribution on similarly located slices of a typical hippocampus in the literature. In Figure 5, all slices from head to tail show the “interlocking C” or the “body-like” profile discovered in (Adler DH et al., 2018; Gross DW et al., 2020). This result shows consensus inner structures along the ARMM long-axis with the manual tracing method. Second, the DG and CA3 serve as pivotal information processing

hubs within the laminar functional units and are likely to be the main drivers of longitudinal information transmission in the hippocampus. For example, the “CA3-centric” viewpoint of hippocampal information processing believes that CA3 pyramidal cells project diversely to all hippocampal principal cells (Scharfman HE, 2007), and many studies have demonstrated the existence of excitatory projecting associational pathways of dentate mossy cells and CA3 pyramidal cells (Gloveli T et al., 2005; Pak S,Jang D,Lee J,Choi G,Shin H,Yang S and Yang S, 2022;Ropireddy D et al., 2011).

Under this long-axis, we are able to construct lamellar architectures in the longitudinal dimension of the hippocampus. Strange BA et al. (2014) suggest that the exact number of domains along the long-axis and whether these domains are hierarchically organized in the human hippocampus is currently unknown. From the gradient perspective, the longitudinal lamella of the hippocampus is expected to be very thin. Mesoscopic level studies have discovered that the longitudinal mossy fibers in the DG-DG connection often stretch up to about 2 mm (Amaral DG and Witter MP, 1989; Pak S et al., 2022), while many other longitudinal connections are shorter. For example, the primary axonal fiber in CA3 producing longitudinal axons towards the subiculum bifurcates often extends up to ~400 μ m (Pak S et al., 2022). In the current study, we generate 23 lamellar domains with 2mm intervals against the long-axis in the results section. Further subdivision of the lamellar domains is available through spoke interpolation. The specific number of lamellar domains should be determined based on the research question and objective.

Morphological correspondence by ARMM

The determination of point-wise correspondence across individuals is a key subject in morphological analysis. Ambiguous correspondences at locations with large individual variabilities may lead to completely different results in statistical analysis. According to (Ding SL and Van Hoesen GW, 2015), the hippocampal head has different numbers of digitations across subjects, posing a major challenge in establishing correspondences. The variability in hippocampal digitations may not be well suited for registration-based approaches, as it is inconclusive how to align the anterior portions among populations with different numbers of digitations (DeKraker J et al., 2021). Furthermore, the correspondence established by current geometric methods is not always directly related to or supported by physiopathological evidence.

Adler discovers that the hippocampal tail (the posterior 1/3 of the hippocampus), while slicing it at approximately 6/9, 7/9, 8/9 of the total hippocampal length along the curvature of the long-axis, very few samples have different subfields distribution (Adler DH et al., 2018). This finding indicates a stable correspondence between individuals along the curved long-axis. Due to difficulties in sample acquisition and manual annotation, evidence for intra-individual correspondence based on the long-axis is rare. At most scenarios, shape changes on the hippocampus of the same individual have little influence on its overall shape, so the internal skeleton of the baseline observation remains stable over time. In section 3.2, we measured local shape variations on time series of hippocampi and find that the focal distribution measured by surface and volumetric features are highly consistent. This finding indirectly verifies the intra-individual correspondence by the long-axis.

However, there remains a limitation for the morphological correspondence by the long-axis. The hippocampus may not undergo isotropic atrophy under the effect of disease.

Therefore, the length and curvature of the long-axis may change, especially in the head and tail of the hippocampus, leading to deviations in the correspondence. As a result, even if the effect is not so extreme, the correspondence established based on proportions is no longer valid. In (Poppenk J et al., 2020), the author describes a similar mis-correspondence example that due to the contraction of the uncus, a larger portion of anterior is redefined as posterior of hippocampus, leading to incorrect conclusion that the posterior segments grow. One possible solution is to use the long-axis of one's healthy hippocampus, and fit the corresponded ARMM coordinates directly to the subject's atrophied hippocampus, followed by eroding extra elements of ARMM outside the boundary surface (i.e., using the longitudinal strategy proposed in *section 2, Model evaluation*).

Limitations and future works

There are some limitations to the current model. First, we restrict the representation of the hippocampus to a single atlas, without validating of the method on the morphology of real hippocampi. We anticipate that it will be possible to further validate the method based on large samples of high-resolution MRI. Second, this model only accommodates a single segmentation protocol, while the diverse protocols for hippocampus segmentation may lead to different long axes and lamellar distributions. We have considered the generality of the long-axis as much as possible by restricting it to the medial surface and moderating extreme lateral/medial curvatures. Future work will further develop and validate the method to accommodate more protocols. Third, the proposed method does not support the representation of subfield morphology within the hippocampus. It would be beneficial to include subfield morphometry in our model, such as subfield shape features on lamellae. Future directions for this work will integrate subfield morphologies for quantitative analysis of subfield variations in aging and neurodegenerative diseases.

5. Conclusions

The conventional tripartite subdivision of the hippocampus into head, body and tail has limited exploration of its underlying mechanisms of longitudinal functional heterogeneity. This paper proposes a novel framework, the axis-referenced morphometric model (ARMM) of the hippocampus, that follows the lamellar organization and enables detailed characterization of anatomically motivated structural features on hippocampal images. The ARMM can measure the hippocampal morphology along its entire long-axis and allows for stable alignment of hippocampi across individuals with variable morphologies using a uniform planar orthogonal coordinate system. The ARMM has been verified to precisely capture the longitudinal hippocampal formation and discover unique features for shape variations due to neurodegeneration. Promising applications of the ARMM include investigation of the longitudinal heterogeneity of the hippocampus and identification of new structural markers for neurodegenerative diseases.

Acknowledgement

This study is supported by grants from the National Natural Science Foundation of P.R. China (62276081, 62106113), Innovation Team and Talents Cultivation Program of National Administration of Traditional Chinese Medicine (NO:ZYYCXTD-C-202004), Basic Research Foundation of Shenzhen Science and Technology Stable Support Program (GXWD20201230155427003-20200822115709001).

Data and Code Availability Statement

The data supporting the findings of this study is based on open-source results from (Adler DH et al., 2018). The data repository is located at <https://www.nitrc.org/projects/pennhippoatlas/>. All code for this project, including the ARMM template, is available at <https://github.com/calliegao/ARMM>. The code for the pipeline will be made publicly available after acceptance.

Reference

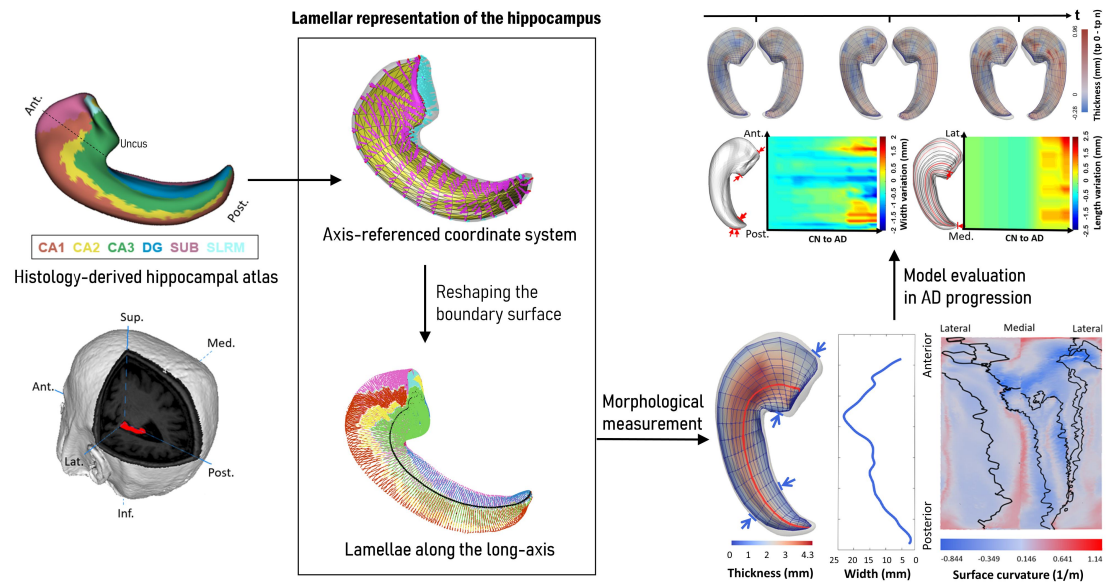
- Adler DH, Wisse LEM, Ittyerah R, Pluta JB, Ding SL, Xie L, Wang J, Kadivar S, et al. (2018), Characterizing the human hippocampus in aging and Alzheimer's disease using a computational atlas derived from ex vivo MRI and histology. Proc Natl Acad Sci U S A 115:4252-4257.
- Amaral DG, Witter MP (1989), The three-dimensional organization of the hippocampal formation: a review of anatomical data. Neuroscience 31:571-591.
- Andersen P, Bliss TV, Skrede KK (1971), Lamellar organization of hippocampal pathways. Exp Brain Res 13:222-238.
- Andersen P, Soleng AF, Raastad M (2000), The hippocampal lamella hypothesis revisited. Brain Res 886:165-171.
- Ayhan F, Kulkarni A, Berto S, Sivaprakasam K, Douglas C, Lega BC, Konopka G (2021), Resolving cellular and molecular diversity along the hippocampal anterior-to-posterior axis in humans. Neuron 109:2091-2105 e2096.
- Baazaoui N, Iqbal K (2022), Alzheimer's Disease: Challenges and a Therapeutic Opportunity to Treat It with a Neurotrophic Compound. Biomolecules 12.
- Bernhardt BC, Bernasconi A, Liu M, Hong SJ, Caldaiou B, Goubran M, Guiot MC, Hall J, et al. (2016), The spectrum of structural and functional imaging abnormalities in temporal lobe epilepsy. Ann Neurol 80:142-153.
- Chauhan P, Jethwa K, Rathawa A, Chauhan G, Mehra S (2021) The Anatomy of the Hippocampus. In: Cerebral Ischemia, vol. (Pluta R, ed). Brisbane (AU).
- Dalton MA, D'Souza A, Lv J, Calamante F (2022), New insights into anatomical connectivity along the anterior-posterior axis of the human hippocampus using in vivo quantitative fibre tracking. Elife 11.
- Dalton MA, McCormick C, De Luca F, Clark IA, Maguire EA (2019), Functional connectivity along the anterior-posterior axis of hippocampal subfields in the ageing human brain. Hippocampus 29:1049-1062.
- Dautricourt S, de Flores R, Landeau B, Poisnel G, Vanhoutte M, Delcroix N, Eustache F, Vivien D, et al. (2021), Longitudinal Changes in Hippocampal Network Connectivity in Alzheimer's Disease. Ann Neurol 90:391-406.
- Decker AL, Duncan K, Finn AS, Mabbott DJ (2020), Children's family income is associated with cognitive function and volume of anterior not posterior hippocampus. Nat Commun 11:4040.
- DeKraker J, Ferko KM, Lau JC, Kohler S, Khan AR (2018), Unfolding the hippocampus: An intrinsic coordinate system for subfield segmentations and quantitative mapping. Neuroimage 167:408-418.
- DeKraker J, Kohler S, Khan AR (2021), Surface-based hippocampal subfield segmentation. Trends Neurosci 44:856-863.
- Ding SL, Van Hoesen GW (2015), Organization and Detailed Parcellation of Human Hippocampal Head and Body Regions Based on a Combined Analysis of Cyto- and

- Chemoarchitecture. *J Comp Neurol* 523:2233-2253.
- Fishbaugh J, Durrleman S, Prastawa M, Gerig G (2017), Geodesic shape regression with multiple geometries and sparse parameters. *Med Image Anal* 39:1-17.
- Genon S, Bernhardt BC, La Joie R, Amunts K, Eickhoff SB (2021), The many dimensions of human hippocampal organization and (dys)function. *Trends Neurosci* 44:977-989.
- Gloveli T, Dugladze T, Rotstein HG, Traub RD, Monyer H, Heinemann U, Whittington MA, Kopell NJ (2005), Orthogonal arrangement of rhythm-generating microcircuits in the hippocampus. *Proc Natl Acad Sci U S A* 102:13295-13300.
- Gross DW, Misaghi E, Steve TA, Wilman AH, Beaulieu C (2020), Curved multiplanar reformatting provides improved visualization of hippocampal anatomy. *Hippocampus* 30:156-161.
- Jinde S, Zsiros V, Nakazawa K (2013), Hilar mossy cell circuitry controlling dentate granule cell excitability. *Front Neural Circuits* 7:14.
- Kalmady SV, Shivakumar V, Arasappa R, Subramaniam A, Gautham S, Venkatasubramanian G, Gangadhar BN (2017), Clinical correlates of hippocampus volume and shape in antipsychotic-naive schizophrenia. *Psychiatry Res Neuroimaging* 263:93-102.
- Kharabian Masouleh S, Plachti A, Hoffstaedter F, Eickhoff S, Genon S (2020), Characterizing the gradients of structural covariance in the human hippocampus. *Neuroimage* 218:116972.
- Langnes E, Sneve MH, Sederevicius D, Amlien IK, Walhovd KB, Fjell AM (2020), Anterior and posterior hippocampus macro- and microstructure across the lifespan in relation to memory-A longitudinal study. *Hippocampus* 30:678-692.
- Lin X, Amalraj M, Blanton C, Avila B, Holmes TC, Nitz DA, Xu X (2021), Noncanonical projections to the hippocampal CA3 regulate spatial learning and memory by modulating the feedforward hippocampal trisynaptic pathway. *PLoS Biol* 19:e3001127.
- Liu Z, Hong J, Vicory J, Damon JN, Pizer SM (2021), Fitting unbranching skeletal structures to objects. *Med Image Anal* 70:102020.
- Pak S, Jang D, Lee J, Choi G, Shin H, Yang S, Yang S (2022), Hippocampal interlamellar cell-cell connectome that counts. *J Cell Physiol* 237:4037-4048.
- Pizer SM, Marron JS, Damon JN, Victory J, Krishna A, Liu Z, Taheri M. (2022), Skeleton, object shape, statistics. *Frontiers in Computer Science* 4:842637.
- Plachti A, Kharabian S, Eickhoff SB, Maleki Balajoo S, Hoffstaedter F, Varikuti DP, Jockwitz C, Caspers S, et al. (2020), Hippocampus co-atrophy pattern in dementia deviates from covariance patterns across the lifespan. *Brain* 143:2788-2802.
- Ropireddy D, Scorcioni R, Lasher B, Buzsaki G, Ascoli GA (2011), Axonal morphometry of hippocampal pyramidal neurons semi-automatically reconstructed after in vivo labeling in different CA3 locations. *Brain Struct Funct* 216:1-15.
- Scharfman HE (2007), The CA3 "backprojection" to the dentate gyrus. *Prog Brain Res* 163:627-637.
- Sloviter RS, Lomo T (2012), Updating the lamellar hypothesis of hippocampal organization. *Front Neural Circuits* 6:102.
- Strange BA, Witter MP, Lein ES, Moser EI (2014), Functional organization of the hippocampal longitudinal axis. *Nat Rev Neurosci* 15:655-669.
- Styner M, Oguz I, Xu S, Brechbuhler C, Pantazis D, Levitt JJ, Shenton ME, Gerig G (2006), Framework for the Statistical Shape Analysis of Brain Structures using SPHARM-PDM. *Insight*

J:242-250.

- Terreros-Roncal J, Flor-Garcia M, Moreno-Jimenez EP, Rodriguez-Moreno CB, Marquez-Valadez B, Gallardo-Caballero M, Rabano A, Llorens-Martin M (2022), Methods to study adult hippocampal neurogenesis in humans and across the phylogeny. *Hippocampus*.
- Vogel JW, La Joie R, Grothe MJ, Diaz-Papkovich A, Doyle A, Vachon-Presseau E, Lepage C, Vos de Wael R, et al. (2020), A molecular gradient along the longitudinal axis of the human hippocampus informs large-scale behavioral systems. *Nat Commun* 11:960.
- Yushkevich PA (2009), Continuous medial representation of brain structures using the biharmonic PDE. *Neuroimage* 45:S99-110.
- Yushkevich PA, Amaral RS, Augustinack JC, Bender AR, Bernstein JD, Boccardi M, Bocchetta M, Burggren AC, et al. (2015), Quantitative comparison of 21 protocols for labeling hippocampal subfields and parahippocampal subregions in vivo MRI: towards a harmonized segmentation protocol. *Neuroimage* 111:526-541.
- Yushkevich PA, Piven J, Hazlett HC, Smith RG, Ho S, Gee JC, Gerig G (2006), User-guided 3D active contour segmentation of anatomical structures: significantly improved efficiency and reliability. *Neuroimage* 31:1116-1128.
- Lee JK, Fandakova Y, Johnson EG, Cohen NJ, Bunge SA, Ghetti S (2020), Changes in anterior and posterior hippocampus differentially predict item-space, item-time, and item-item memory improvement. *Dev Cogn Neurosci* 41:100741.
- Small SA, Schobel SA, Buxton RB, Witter MP, Barnes CA (2011), A pathophysiological framework of hippocampal dysfunction in ageing and disease. *Nat Rev Neurosci* 12:585-601.
- Szeszko PR, Goldberg E, Gunduz-Bruce H, Ashtari M, Robinson D, Malhotra AK, Lencz T, Bates J, et al. (2003), Smaller anterior hippocampal formation volume in antipsychotic-naive patients with first-episode schizophrenia. *Am J Psychiatry* 160:2190-2197.
- Meng T W, Pui-Tung Choi G , Lui L M . (2016) TEMPO: Feature-Endowed Teichmüller Extremal Mappings of Point Clouds[J]. *Computer ence* 9(4):1922-1962.
- Poppenk J, Alzheimer's Disease Neuroimaging Initiative HCP, Cambridge Centre for A, Neuroscience (2020), Uncal apex position varies with normal aging. *Hippocampus* 30:724-732.
- Irving AJ, Harvey J (2014), Leptin regulation of hippocampal synaptic function in health and disease. *Philos Trans R Soc Lond B Biol Sci* 369:20130155.
- Noh W, Pak S, Choi G, Yang S, Yang S (2019), Transient Potassium Channels: Therapeutic Targets for Brain Disorders. *Front Cell Neurosci* 13:265.
- Pak S, Jang D, Lee J, Choi G, Shin H, Yang S, Yang S (2022), Hippocampal interlamellar cell-cell connectome that counts. *J Cell Physiol* 237:4037-4048.
- Siddiqi, Kaleem, Pizer, Stephen M., 2008. Medial Representations. Springer Netherlands.
- Cignoni P., Callieri M., Corsini M., Dellepiane M., Ganovelli F., Ranzuglia G. (2008) MeshLab: an Open-Source Mesh Processing Tool. Sixth Eurographics Italian Chapter Conference, page 129-136, 2008
- Jones, S.E., Buchbinder, B.R., et al., 2000. Three-dimensional mapping of cortical thickness using Laplace's equation. *Human Brain Mapping* 11, 12-32.

Figure Legends



Graphic abstract

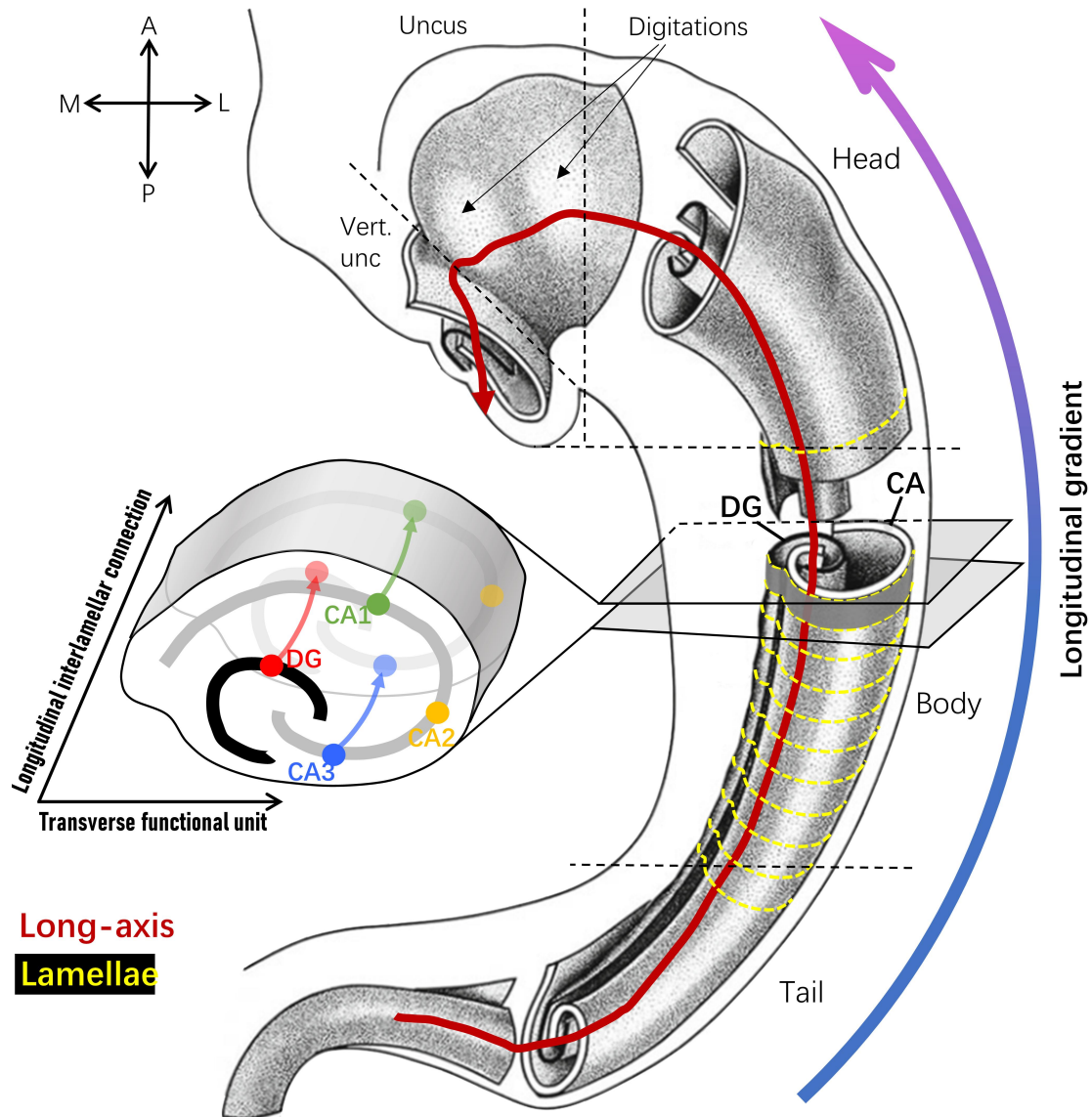


Figure 1. Anatomical longitudinal organization of the hippocampus. The CA and DG form an "interlocking C" profile on each lamella along the entire long-axis. Each lamellar slice contains a transverse functional unit across DG (red), CA1 (green), CA2 (orange) and CA3 (blue). Longitudinal interlamellar connection, dominated by mossy fibers and granule cells in DG and pyramidal cells in CA3 and CA1, are intensively existed along the long-axis. The strip-formed lamellar structure (yellow) is distributed nearly perpendicular to the long-axis of the hippocampus (crimson). Functional and anatomic connectivity with extra-hippocampal structures shows a gradient along the longitudinal dimension (Anterior, magenta; dark blue, posterior). Abbreviations: CA, cornu ammonis; DG, dentate gyrus; SUB, subiculum; SRLM, stratum radiatum lacunosum moleculare; EC, entorhinal cortex; A, anterior; P, posterior; L, lateral; M, medial. Vert. unc, vertical uncus.

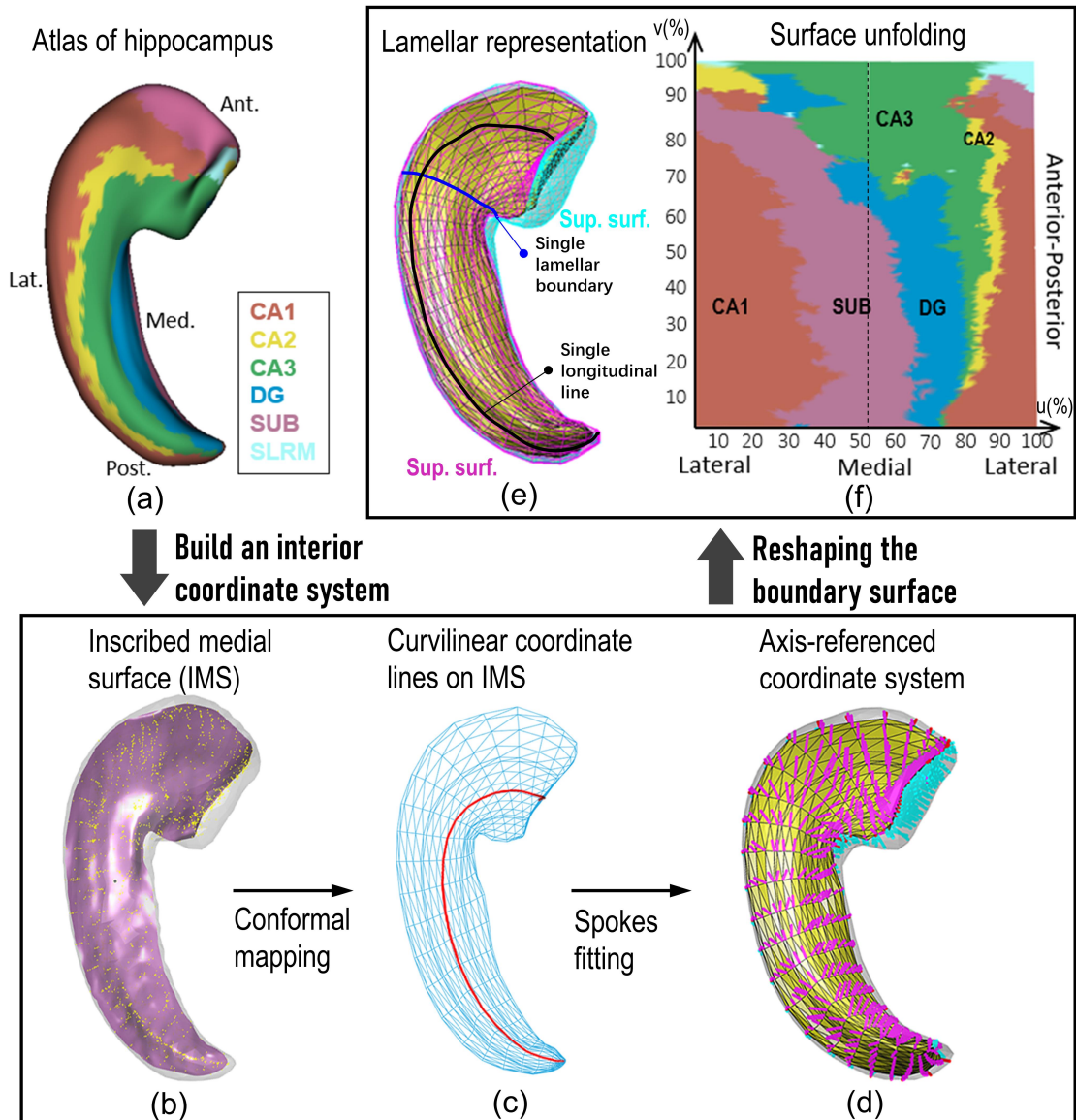


Figure 2. The methodological framework of ARMM. A hippocampal boundary surface (a) is first extracted from MR image. b) The surface is then used to calculate the IMS (pink) by NURBS surface fitting with Voronoi graph vertexes (yellow) that generate from the hippocampal boundary surface mesh. The blue mesh in (c) is a reparameterized IMS, with the centermost axis (red) manually fitted to be generally agree with the CA-DG border of the hippocampus. (d) Spokes calculated according to geometric constrains on IMS (yellow) and boundary surface. The superior and inferior spokes, colored in magenta and cyan respectively, pointing from the IMS to the gray boundary surface. (e) a hippocampal surface with transversal lamellar and longitudinal axes is generated from the IMS and spokes. Note that the boundary surface is composed of the superior and inferior parts colored in magenta and cyan respectively. Abbreviations: IMS, inscribed medial surface; CA, cornu ammonis; DG, dentate gyrus; SUB, subiculum; SRLM, stratum radiatum lacunosum moleculare; Ant, anterior; Post, posterior; Lat, lateral; Med, medial.

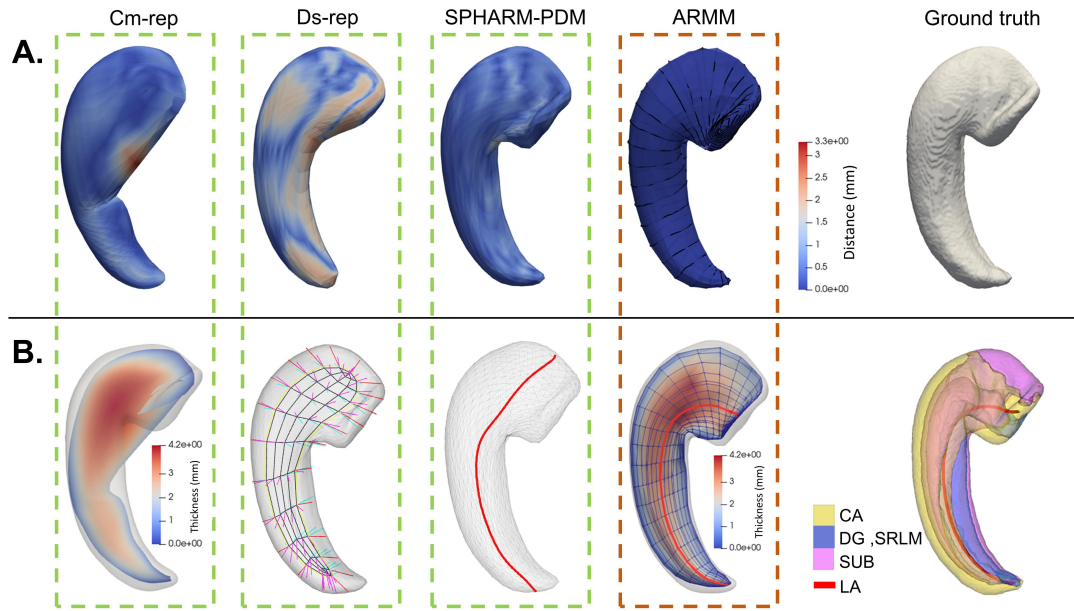


Figure 3. Comparisons of the four hippocampal shape models. A) Point-wise distance maps of the models. The locations colored in red denote large errors between the ground truth surface and the reconstructed surfaces by the shape models. B) Axes generated from the four models. In the last panel, the long-axis generated from ARMM is visualized inside the 3D hippocampus. Abbreviations: CA, cornu ammonis; DG, dentate gyrus; Sub, subiculum; LA, long-axis.

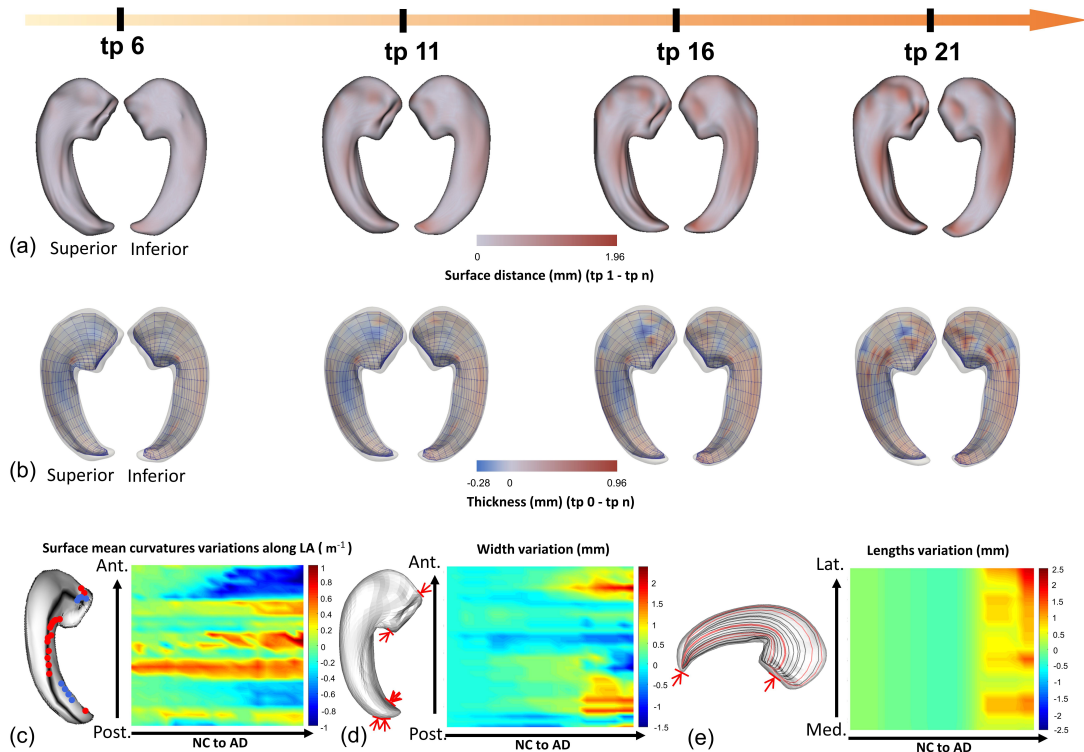


Figure 4. Morphological features calculated from the ARMM and measurement of local shape variations on a time series of left hippocampi. a) Local surface variations on the superior and inferior parts of the hippocampus at four selected time points. Surface

contraction indicated focal atrophy is colored in red. b) Local thickness variations on the superior and inferior parts of the hippocampus at four selected time points, where thickness decrease is colored in red. c) Typical local surface curvature variations along the longitudinal axis. Curvature decreases/straightening (red); curvature increases/bending (blue). d) Hippocampal width variation along the long-axis (from posterior to anterior). Typical atrophy locations, where width decrease compared to the baseline, are denoted by red arrows. e) Hippocampal length variations along transverse axes during AD progression. Note that the color red in all color bars denotes decreases of the measurements compared to the baseline, while blue denotes the increase of the measurements. Abbreviations: tp, time point; LA, long-axis; NC, nondementia control; AD, Alzheimer's disease.

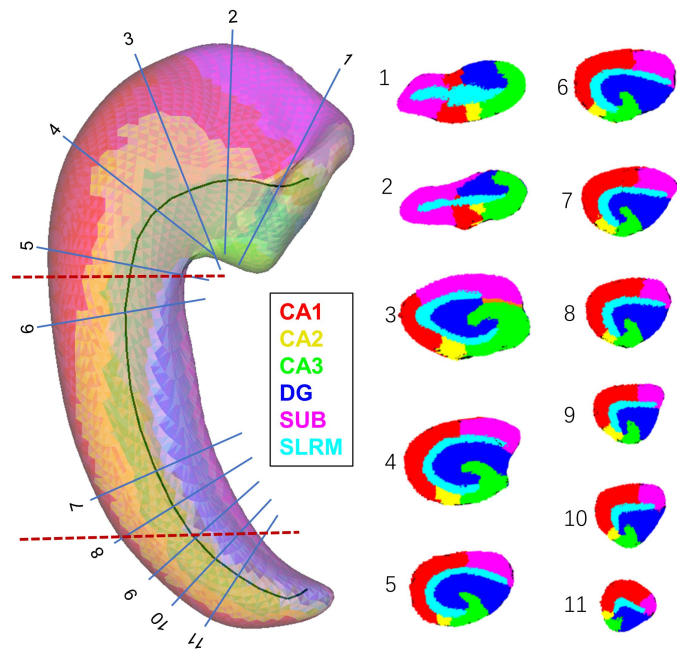


Figure 5. Representative slices that cut perpendicularly to the ARMM-derived long-axis. Left: traditional subdivision method (red dotted lines) and slicing along directions perpendicular to the long-axis (blue lines). Right: Slices corresponding to the cutting orientations shown in the left panel.

Table 2. Shape errors between each reconstructed shape and the ground truth.

<i>Portions of hippocampus</i>	<i>Shape similarity metrics</i>	ARMM	Cm-rep	SPAHRM	Ds-rep
<i>Whole hippocampus</i>	<i>Surface distance (mm)</i>	0.0003	0.0071	0.0012	0.026
	<i>Areal difference (mm²)</i>	1.2404	0.4222	1.7255	9.9669
	<i>Curvedness error (1/mm)</i>	0.0133	5.0635	0.0326	0.0592
	<i>Dice</i>	0.9961	0.8313	0.9702	0.9074
<i>Head</i>	<i>Surface distance (mm)</i>	0.0002	0.0054	0.0009	0.0028
	<i>Areal difference (mm²)</i>	0.5217	7.4814	1.5972	11.3964
	<i>Curvedness error (1/mm)</i>	0.002	6.9358	0.0293	0.0643
	<i>Dice</i>	0.9959	0.8277	0.9732	0.9045
<i>Head fold</i>	<i>Surface distance (mm)</i>	0.0003	0.0069	0.001	0.0044
	<i>Areal difference (mm²)</i>	0.6414	1.2509	1.3612	17.8808
	<i>Curvedness error (1/mm)</i>	0.0024	14.136	0.0224	0.0573
	<i>Dice</i>	0.9934	0.6815	0.9706	0.8459
<i>Body</i>	<i>Surface distance (mm)</i>	0.0004	0.0106	0.0012	0.1137
	<i>Areal difference (mm²)</i>	0.1076	8.1713	0.127	5.4684
	<i>Curvedness error (1/mm)</i>	0.0679	0.0281	0.0134	0.0146
	<i>Dice</i>	0.998	0.8403	0.9722	0.9284
<i>Tail</i>	<i>Surface distance (mm)</i>	0.0002	0.0046	0.0012	0.0031
	<i>Areal difference (mm²)</i>	0.2534	17.5162	2.0229	10.8307
	<i>Curvedness error (1/mm)</i>	0.0029	0.0095	0.0402	0.0501
	<i>Dice</i>	0.997	0.8313	0.9611	0.8934
<i>Tail tip</i>	<i>Surface distance (mm)</i>	0.0004	0.008	0.0017	0.0061
	<i>Areal difference (mm²)</i>	0.3948	28.8729	4.0824	25.5454
	<i>Curvedness error (1/mm)</i>	0.0036	0.0445	0.0369	0.0037
	<i>Dice</i>	0.9939	0.7272	0.9517	0.7747